NDT&E International 133 (2023) 102760

Contents lists available at ScienceDirect

NDT and E International

journal homepage: www.elsevier.com/locate/ndteint

Pressure monitoring of Special Nuclear Material containment☆

Elizabeth H. Sharp [a,*], Robert Bernard [b], Gary Bolton [c], Steve Dixon [a]

[a] University of Warwick, Gibbet Hill Road, Coventry, CV47AL, United Kingdom
[b] Sellafield Limited, Sellafield, Seascale, CA201PG, United Kingdom
[c] National Nuclear Laboratory, Birchwood Park, Warrington, WA36AE, United Kingdom

ARTICLE INFO

Keywords:
Pressure monitoring
Special Nuclear Material
Electromagnetic acoustic transducer
Frequency analysis

ABSTRACT

All Magnox Nuclear Reactors are now in the process of decommissioning and nearly all Magnox spent fuel has been reprocessed, producing uranium and plutonium and small volumes of highly radioactive waste. The recovered plutonium is stored in specialist containers in secure facilities while the government reaches a decision on possible re-use or disposal, following the completion of technical studies. There is potential for the containment to become pressurised over time due to alpha decay and radiolysis of the plutonium, and highlights the need for continuous monitoring to assess the integrity of the containment. This paper presents a new technique of interpreting the internal pressure of the containment by understanding the change in the vibrational response of the outer containment wall for different internal pressures. Electromagnetic acoustic transducers have been used to excite the outer containment wall in a non-contact and non-destructive manner, and capture the changes in the resonant frequency response of the system for different internal pressures.

1. Introduction

Nuclear power stations have been utilised in the UK for many decades, since 1956 when the UK became the first country to supply electricity from a commercial nuclear power station, Calder Hall, situated in Cumbria. Over time, the nuclear industry has grown significantly, and now many nuclear power stations are in operation, contributing to around 18% of the country's electricity produced [1]. Many non-power producing facilities are in operation that are critical to maintaining the nuclear industry including facilities to support the nuclear fuel cycle such as, fuel production and reprocessing, and management of waste and radioactive material [2].

All first generation Magnox nuclear reactors have reached the end of their operating life and are in the process of being defuelled, ready for decommissioning. The spent fuel from the Magnox fleet of reactors has been reprocessed at the Magnox Reprocessing Plant on the Sellafield site. Reprocessing extracts nuclear materials (plutonium and uranium) that could potentially be re-used and also generates 'fission products' which are managed as highly radioactive waste [2,3]. In the UK, the Nuclear Decommissioning Authority (NDA), a government body that was set-up in 2004, is responsible for the clean-up of the UK's early nuclear sites safely. The NDA strategy for nuclear materials is to ensure safe, secure and cost-effective lifecycle management of nuclear materials [4]. All nuclear materials will be either converted into new fuel for nuclear reactors or immobilised and stored until a permanent UK disposal facility is developed. Plutonium, the focus of this paper, is consolidated in packages as plutonium oxide (PuO_2) suitable for long term storage while the government reaches a decision on possible re-use or disposal [5]. The PuO_2 is allocated to a type of Special Nuclear Material (SNM) containment, denoted as Magnox packages, comprising an Aluminium inner container, a polyethylene intermediate container and a welded outer 316L stainless steel canister [6]. These vessels are then transferred to secure interim storage facilities awaiting government's decision on re-use or disposal.

The storage of Magnox packages has presented a new challenge that needs addressing. Internal radiation chemistry attributed to PuO_2 is known to potentially cause issues that lead to concerns over package integrity and safety for long-term storage. The packages can develop higher internal pressure because of the production of hydrogen and helium from radiolysis and alpha decay, respectively [6,7]. Visible degradation to several of the packages within the interim storage facilities have been reported, such as bulging on the base and top of the packages. Therefore, it is critical that the current stockpile of Magnox packages are monitored regularly. The issue becomes more complex, as the radiolysis reaction is a cyclic process that can cause pressurisation

☆ This work was supported by the Nuclear Decommissioning Authority (NDA), United Kingdom and the National Nuclear Laboratory (NNL) under grant NNL/UA/071.

* Corresponding author.
E-mail addresses: elizabeth.sharp@warwick.ac.uk (E.H. Sharp), robert.bernard@sellafieldsites.com (R. Bernard), gary.bolton@uknnl.com (G. Bolton), s.m.dixon@warwick.ac.uk (S. Dixon).

https://doi.org/10.1016/j.ndteint.2022.102760
Received 23 August 2022; Received in revised form 23 September 2022; Accepted 17 October 2022
Available online 29 October 2022

and depressurisation of the package over long periods of time, making it difficult to determine an accurate measurement of internal pressure using current inspection techniques.

Before packages are placed into the storage facility, the length of each can is measured and used as a reference for future measurements. Within some of the storage facilities the preferred method of package inspection is laser distance measurements. A port profiler traverses the channels in which the packages are stored and the length of each containment is collected. An internal pressure measurement is then estimated from the resulting containment length. The inspection technique presents multiple limitations; measurements are associated with a large margin of error and in the case where the package has undergone plastic deformation, the length measurement is no longer reliable if depressurisation has occurred. These limitations highlight the significance of developing a technique that can accurately determine the internal pressure of the SNM containment within the storage facility. However, special considerations are required when considering an alternative inspection technique. Access to each container in the storage facility is restricted, and makes larger devices impractical. High levels of radiation, temperature and humidity are also of concern, and result in a large proportion of techniques further being disregarded as an option.

Consideration has been given to using electromagnetic acoustic transducers (EMATs), for the non-contact, acoustic and ultrasonic testing of the containers. EMATs do not require mechanical coupling, such as liquid or solid polymer couplant, to generate or detect vibrations in a conducting surface and are therefore classified as non-contact transducers. In practical use, they are often used close to, or in light contact with the sample surface as this makes sensor delivery easier and does not affect the measurement being made. EMATs can be held off at small distances from a sample surface when required, resulting in a strictly non-contact transducer method with a decrease in generation and detection efficiency [8,9]. EMATs can generate or detect ultrasonic or acoustic waves of the surface of an electrically conducting material. Their low cost, small size and durability at elevated temperatures makes them attractive for various applications [10]. Previous research has demonstrated the successful use of EMATs within the field of non-destructive testing (NDT) for various applications, such as stress measurements, grain size measurements and texture measurements of metal sheets [11–13]. When using EMATs, the inspected material must be electrically conductive, such that low conductivity materials lead to poor transduction efficiency of EMATs, resulting in a poor signal-to-noise ratio when compared to piezoelectric ultrasonic transducers. This paper presents the use of a wideband, self-field EMAT [14] to excite the vibrational modes of the conductive outer Magnox container, and a linear coil EMAT to detect the resulting excited vibrational modes. Microphone measurements have also been conducted, to compare the air-borne acoustic displacements emitted from the containment wall to the out-of-plane material displacements of the package wall detected by the EMAT.

2. Vibrational response

The vibrational response of a system is correlated to its oscillatory behaviour, and requires that the system has inertia to transfer momentum, and elasticity that allows the system to return to equilibrium [15]. The preferential vibrational modes at which a system oscillates during free vibration, are known as the natural or resonant frequencies of the system, and are defined by particular frequency values. The shape in which the structure vibrates is known as the mode shape and corresponds to a particular resonant frequency. The resonant frequencies and associated mode shapes of a system depend upon the physical properties of the system, such as, mass, elasticity, and boundary conditions. Therefore, the frequency spectrum of a system is specific to that system only, and acts as a fingerprint for its vibrational response.

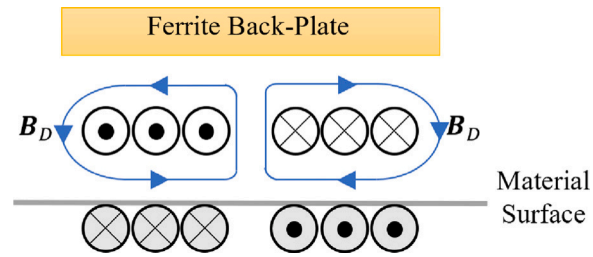

Fig. 1. Cross-sectional view of the self-field spiral coil and the generated eddy current within the surface of the material. Ferrite back-plate and coil are separated to demonstrate the dynamic magnetic field B_D around each coil section.

Within NDT, multiple techniques have utilised the resonant frequency spectrum of a system as a baseline for inspection measurements. The measurable change in the resonant frequencies of a system due to some external influences have been investigated in the published literature, and show capabilities for stress measurements and creep damage assessment of materials. Hirao and Ogi's [11] work on electromagnetic acoustic resonance (EMAR), outlines a method for acoustoelastic stress measurement of a metal plate by measuring the frequency shift of three specific resonant frequencies. Similarly, Ohtani et al. [8] have investigated the effects of creep damage in ferritic steel by examining a range of resonance frequencies and the attenuation of a particular mode during each creep test.

The work presented in this paper investigates changes to the vibrational response of the Magnox containment at different internal pressures. The approach used is similar to the previous works mentioned [8,11]. Vibrational resonant frequencies below 10 kHz have been identified from the frequency spectrum of the Magnox containment at atmospheric pressures, and have been used as a benchmark measurement when comparing to other spectra for increasing package pressure. Multiple vibrational modes have been isolated and tracked through the frequency spectra, over the measured internal pressure range of 1 to 20 Bar. Results have shown that there is a correlation between the increasing internal pressure of the containment and the frequency shift of multiple vibrational resonant frequencies. The techniques used within this work have demonstrated the capability of the approach for measuring the internal pressure of the SNM containment, via measuring changes in the containment's vibrational response with changes in internal pressure.

3. Experimental procedure

Measurements were taken on a slightly deformed Magnox containment vessel, which was filled with silver sand and stainless steel shot, to simulate the typical mass of the material usually stored in the package. The dimensions of the Magnox sample cannot be disclosed within this paper for security reasons. However, schematic diagrams of the experimental set-up have been included, in order to provide a basic understanding of the sample geometry. The outer containment wall of the sample is made of 316L stainless steel, that is used due to its corrosion resistance and non-magnetic properties. It should be noted that the stainless steel shot mass simulant used was slightly magnetic, but this should have no significant affect on the operation of the EMATs.

3.1. EMAT generation and detection

The EMAT generator used in this work was constructed from 22 turns of 0.25 mm diameter insulated copper wire, producing a spiral shaped pancake coil that was driven with a pulsed current source of 400 A peak amplitude, with a rise time of 2.6 μs. Previous work has shown that eddy current and ultrasonic generation efficiency can

be significantly enhanced when using a ferrite back-plate behind the inductor coil [16]. Hence, a 4.5 mm thick and 22 mm diameter ferrite disc was placed 1 mm behind the inductor coil as shown in Fig. 1.

When driving a coil-only EMAT with a transient current pulse in the presence of a conducting material, the time varying magnetic field produced by the coil induces an eddy current density within the material surface. For an electromagnetic plane wave, the depth into the sample which the eddy current density is generated is characterised by the electromagnetic skin depth [9]:

$$\delta = \sqrt{\frac{2}{\omega \eta \mu_0 \mu}} \tag{1}$$

where δ is the skin depth, ω is the angular frequency, η, the electrical conductivity, μ and μ_0 the relative permeability and permeability of free space respectively. Note that for a realistic, finite sized EMAT coil, the electromagnetic wave is not planar, but this discussion promotes an indication of the general behaviour and the physics involved. The eddy currents within the material interact with the dynamic magnetic field from the EMAT and the electrons within that current impart momentum to the atoms in the material, resulting in a generated body force. This force is characterised as a Lorentz force which is defined by the equation [8]:

$$\mathbf{F}_L = \mathbf{J} \times \mathbf{B_D} \tag{2}$$

where $\mathbf{F}_L$ is the generated Lorentz force, $\mathbf{J}$ is the eddy current density, and $\mathbf{B_D}$ is the dynamic magnetic field density. As a result of the coil geometry, a radial dynamic magnetic field is generated that is parallel to the sample surface, and gives rise to predominantly longitudinal force components that act normal into the surface of the material. As a result of the longitudinal generated force components, the detection EMAT was constructed such that it is sensitive to the out-of-plane surface displacements of the can wall. The process of detecting elastic wave vibrations at the surface of a material follows the reverse process of the generation mechanism [9]. A 30 mm length and 5 mm wide linear coil was wound centrally around three stacked Neodymium (NdFeB) magnets, which provided significant in-plane static magnetic field components to achieve motion sensitivity in the out-of-plane direction, as shown in Fig. 2. The combination of the material in motion while in the presence of the static magnetic field, results in dynamic currents being induced in the sample material. This induces a potential difference across the detection EMAT coil. The use of multiple magnets offers the benefits of increased magnetic flux density within the material and a greater linear magnetic field region, enhancing the detection of elastic waves. In many cases the detection EMAT is constructed such that particular wave modes can be preferentially detected [9]. However, there is no requirement to configure a specific coil design, as we are detecting a range of vibrational frequencies of the containment wall.

Fig. 3 shows the placement of the EMATs on the SNM package. The generation and detection EMATs were placed at the midpoint of the can wall, with 180° separation around the circumference of the can. The package was pressurised using the connected pressure line, with acoustic measurements being taken at intervals of 0.2 Bar, from atmospheric pressure to 20 Bar. The generation EMAT was used to excite the vibrational frequencies of the SNM package at each pressure interval, while the receive EMAT detected the out-of-plane displacements of the can wall over a period of time, after the generation EMAT was triggered. The received signals were passed through a low frequency EMAT amplifier (see Fig. 5), such that the amplitude-time signal was amplified by a gain of 40 dB and a low pass filter was applied to reduce frequencies above approximately 50 kHz, although filtering is not essential as the data is processed by a fast Fourier transform. An oscilloscope (Tektronix DPO Series Oscilloscope) was used to display the receive signal at each measured pressured interval (see Fig. 5), and any data acquisition hardware could have been used with a suitable acquisition rate and bandwidth.

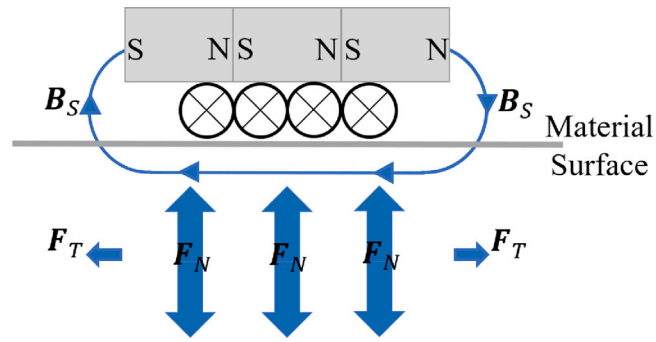

Fig. 2. Schematic of linear coil receive EMAT with three stacked magnets that provides a tangential magnetic field, $\mathbf{B}_S$, through the surface of the containment wall. This configuration enables detection of normal forces, $\mathbf{F}_N$, and a very small contribution of tangential forces, $\mathbf{F}_T$.

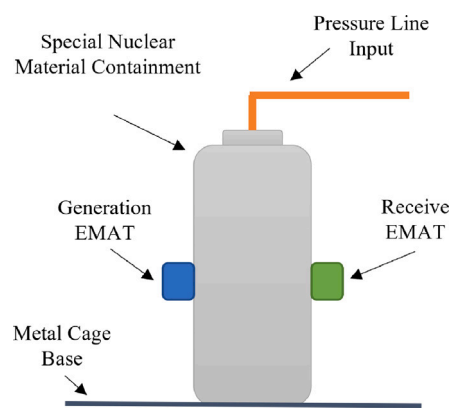

Fig. 3. Schematic diagram of the EMAT generation and detection set-up inside metal safety cage. The generation and detection EMAT's were placed at the midpoint of the outer containment wall with 180° separation around the circumference. The generation EMAT excites the vibrational modes of the outer containment wall and the out-of-plane displacements are detected by the detection EMAT.

3.2. Microphone detection

An alternative detection method was used during the experimental work to compare with the findings from the EMAT receiver. A calibrated pressure field microphone (Brüel & Kjær 4138A-015) was used to measure the air-borne acoustic displacements generated by the containment wall vibrations, after excitation by the generation EMAT at each pressure interval. A schematic diagram of the experimental set-up for the microphone detection method is shown within Fig. 4. The microphone was placed a few centimetres from the midpoint of the can wall, with 180° separation between the generation transducer and the Microphone. Both detection methods were used simultaneously during the experimental work.

4. Results and discussion

4.1. EMAT generation characteristics

The range of resonant modes of the SNM containment that can be excited is dependent upon the excitation frequencies from the generation EMAT, the EMATs location on the containment wall, the size of the generation coil and the coil lift off. The frequency content is determined by the temporal width of the drive current pulse used. The drive current profile was measured by placing a non-inductive 0.1 Ω resistor in series with the EMAT coil, when driven with a wideband high power EMAT pulser. The voltage across the resistor was recorded and Ohm's law

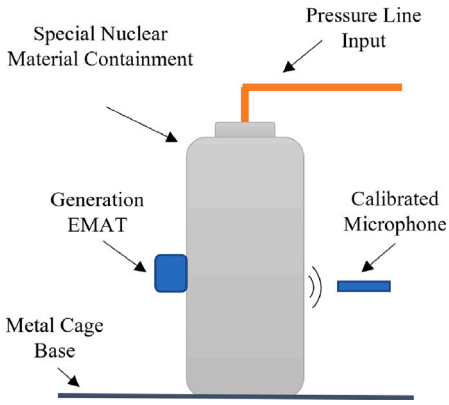

Fig. 4. Schematic diagram of the EMAT generation and microphone detection set-up inside the metal safety cage. The generation EMAT was placed at the midpoint of the outer containment wall with 180° separation from the microphone. The generation EMAT excites the vibrational modes of the outer containment wall and the air-borne acoustic displacements are detected by the microphone.

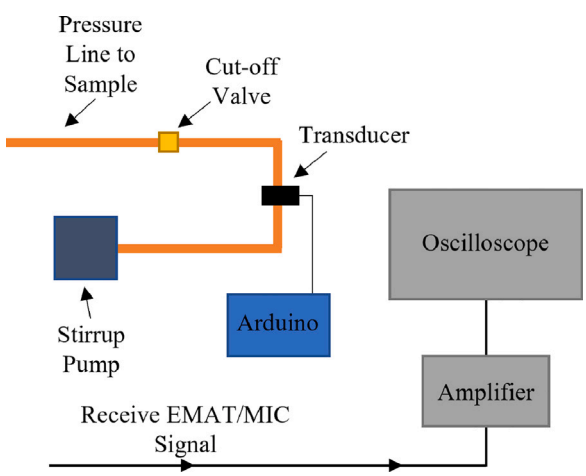

Fig. 5. Schematic diagram of equipment external to the metal safety cage. The SNM package is pressurised by a stirrup pump, an Arduino [17] is used to calculate and read the internal pressure measurement from the inline transducer. The output signals from the EMAT and microphone are amplified and displayed on an oscilloscope.

was used to calculate the current. The peak current amplitude was calculated to be 337 A (Fig. 6) with a rise time of approximately 2.6 μs.

The frequency content of the drive current profile was examined by application of a magnitude Fast Fourier Transform (FFT) in Matlab [18]. Inspection of Fig. 7 shows that the generation EMAT delivers a broadband excitation up to 200 kHz, with the bulk of the frequency content at approximately 20 kHz. A large proportion of the vibrational frequencies that are excited are within the acoustic and low ultrasonic region. Using Eq. (1), the skin depths for 20 kHz and 200 kHz are calculated to be 3.05 mm and 0.96 mm, respectively, meaning a range of surface to bulk forces are imparted on the containment wall [9]. The effect of lift-off can be considered minimal, as the generation EMAT was placed directly in contact with the outer containment wall.

4.2. Vibrational response analysis

The vibrational response of the Magnox containment was obtained by post-processing the amplitude–time signals in Matlab [18]. A Hanning window was applied to each signal to minimise the contribution of the excitation pulse in the frequency responses, as this is generally picked up as electromagnetic noise. The windowed signals were then zero-padded and the vibrational frequency content at each pressure

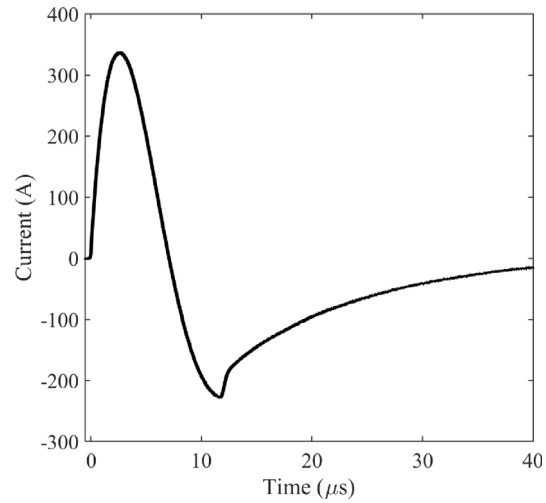

Fig. 6. Excitation current pulse delivered to EMAT coil with a peak value of approximately 337 A.

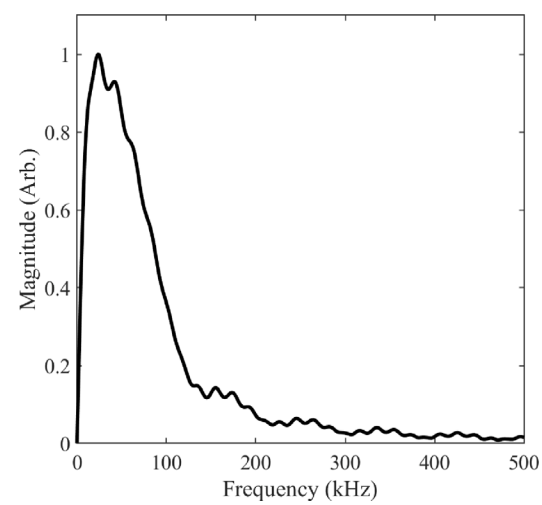

Fig. 7. Fast Fourier transform of the drive current showing the range of frequencies for the outer containment that can be excited. Note that the temporal of time window in Fig. 6 limits the reliability of any low frequency information in the FFT, even though there is still significant frequency content below 20 kHz.

interval was calculated by application of an FFT to the time domain data. The resulting frequency spectra were arranged to produce a normalised magnitude spectra array, each row of the array corresponding to a pressure value. The 'imagesc' function in Matlab [18] was used to display the spectra array data as an image plot with a scaled colour bar. The number of rows and columns of the spectra array corresponds to the number of pressure intervals and frequency steps, respectively. An image plot is produced with frequency on the x-axis, pressure on the y-axis and the normalised magnitude range of the spectra array is represented by the colour bar.

The receive EMAT detected vibrational frequencies up to approximately 60 kHz. However, the range of frequencies chosen to be investigated were within the low acoustic region, at 10 kHz and below. Fig. 7 shows that below 20 kHz, the magnitude of the frequencies drops off quickly and points to the low acoustic region having very little energy. However, this is a limitation of the FFT when using a short time window in comparison to the time periods of the very low frequency components of the spectrum. It is something to be cautious of when analysing the data. In the low acoustic region, the vibrational frequency peaks are more clearly spaced and easier to track over a range of

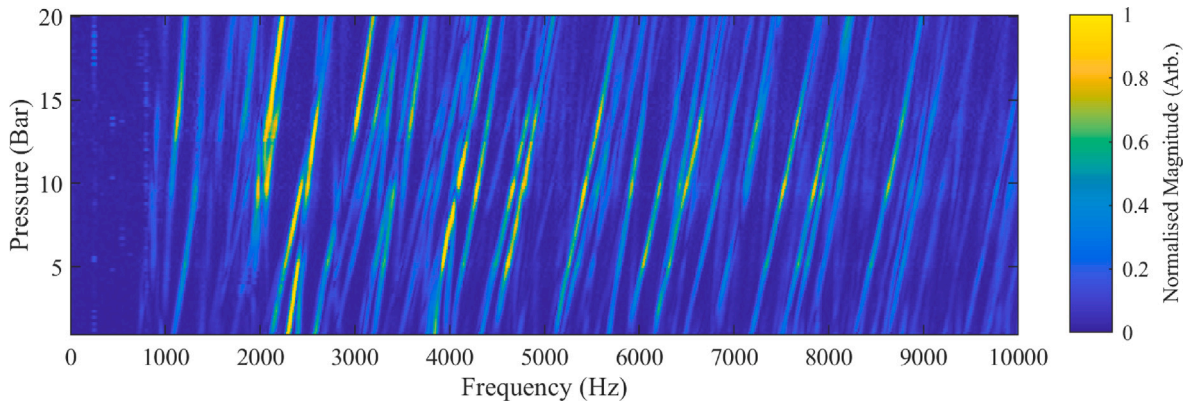

Fig. 8. Image plot of the spectral response of the Magnox containment when the detection EMAT is used to record the out-of-plane displacements of the containment wall. (For interpretation of the references to colour in this figure legend, the reader is referred to the web version of this article.)

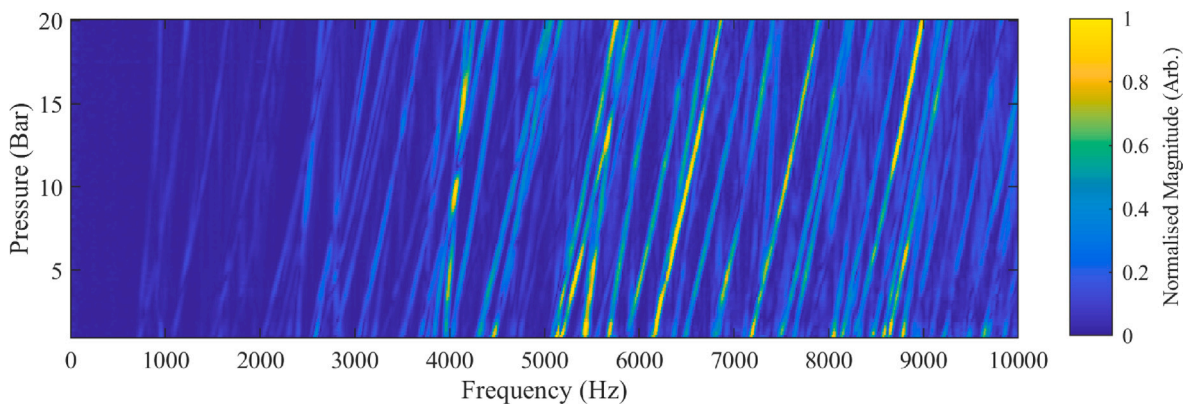

Fig. 9. Image plot of the spectral response of the Magnox containment when the microphone is used to record the air-borne acoustic displacements emitted from the containment wall.

pressures, compared to the higher frequency regions where peaks are very close together and are difficult to isolate. Fig. 8 shows the image plot when using the receive EMAT to detect the out-of-plane displacements of the containment wall. The vibrational resonant frequencies are identified by colours on the colour bar that show considerable contrast against the dark-blue background of the image plot. The dark blue colour represents the low magnitude components of the spectra and is analogous to the noise in a frequency–magnitude plot. The colours that present reasonable contrast against the low frequency components of the spectra, are light-blue to yellow, and represent the larger magnitude components of the spectra, which are indicative of vibrational resonant frequencies. Many vibrational resonant frequencies are observed in the image plot at atmospheric pressure from 0–10 kHz. As the internal pressure of the Magnox containment increases, the same frequencies identified at atmospheric pressure are now shown to shift to the right of the spectra with increasing pressure, showing an increase in their frequency values.

Fig. 9 shows the image plot when using the microphone to detect the air-borne acoustic displacements emitted from the containment wall. The microphone results confirm the findings shown in the EMAT results. There is a clear shift in the vibrational resonant frequency values for increasing internal pressure of the Magnox can. As stated in Section 2, the resonant frequencies of a system are correlated to its elastic properties and this link has been utilised in many studies. It appears from the image plots shown, that as the internal pressure of the Magnox can increases, it is reasonable to assume that the stiffness of the Magnox can wall material increases, resulting in an increase in the vibrational resonant frequency values detected.

Figs. 10 and 11 show the reduced frequency range image plots for the EMAT and microphone detection methods, respectively. The dynamic range of the normalised magnitude colour bar has been adjusted for each plot to enhance the features below 3 kHz, that are not as prominent within the full range image plots. The normalisation process is one limitation when using image plots, normalising the spectral magnitudes against the largest frequency component within the spectra results in some frequencies appearing less prominent within the spectra when displaying them in this way. However, adjusting the frequency range of the image plot and the dynamic range of the normalised magnitude colour bar, additional vibrational resonant frequencies can be identified, with a very good signal to noise ratio.

The resonant frequency variation of two separate isolated modes, have been extracted from the EMAT and microphone image plots. Fig. 12 shows the resonant frequency variation of the first isolated mode as a function of pressure, measured at 4472 Hz and 4466 Hz (±1.39) at atmospheric pressure (±0.01), by the EMAT and microphone respectively. The measured resonant frequency values for the EMAT and microphone are very similar across the full pressure range, with some values agreeing for both detection methods, for instance from 9 to 10 Bar. Occasionally, there are some variations between the measured frequency values, especially in the higher pressure region of 15 Bar and upwards. When using a Fast Fourier Transform to convert time data into the frequency domain, resonant frequency values extracted from the spectra should be viewed with some caution. Dixon et al. [19] have shown that there is some degree of variability in the peak positions calculated when using an FFT when compared to actual resonant frequencies. This is a problem inherent in the FFT calculation itself, due to multiple wave frequency contributions in the magnitude term of the calculation. This results in some peak position variation, due to the interference in the FFT of different frequencies present in the time domain data that are close to each other. The contribution of these variations to the measured frequency values by the EMAT

and microphone are reasonably small, when compared to the peak frequency position shifts for increasing internal pressure of the Magnox packages.

In Matlab [18] the 'fitlm' function was used to apply a linear regression fit to both the EMAT and microphone isolated mode plots. The calculated standard deviation of the residuals was 0.19 and 0.33 Bar for the EMAT and microphone measurements, respectively. The low standard deviation values highlight that the generated fit by the model closely follows the experimental data. In this case, it is reasonable to assume that the relationship between pressure and the resonant frequency shift of the mode is linear. Thus, the calculated gradient of each fit quantifies the Bar/Hz shift of the mode. The gradient calculated for the EMAT fit was 0.032 Bar/Hz with a standard error of 0.000146 Bar/Hz, and for the microphone fit, 0.032 Bar/Hz with a standard error of 0.000267 Bar/Hz. As both fits have produced an equivalent gradient with low standard error values, it suggests that there is good agreement between each detection method and both are suitable for inferring a pressure measurement of the SNM containment when monitoring the shift of resonant frequency modes.

Another mode was analysed and is shown in Fig. 13. The resonant frequency variation of the second isolated mode as a function of pressure was plotted, and was measured at 6163 Hz and 6155 Hz at atmospheric pressure, by the EMAT and microphone respectively. The measurement uncertainties remain the same as previously stated. There appears to be clear similarities between the EMAT and microphone measured resonant frequency values across the full pressure range with very little variation. A linear regression fit was applied to both the EMAT and microphone mode plots and the standard deviation of the residuals were calculated. The calculated standard deviation of the residuals were 0.22 and 0.20 Bar for the EMAT and microphone, respectively. Assuming a linear relationship between pressure and the resonant frequency shift of the mode, the gradient of each fit was calculated and provided a measurement for the Bar/Hz shift of the mode. The gradient of the EMAT fit was 0.028 Bar/Hz with a standard error of 0.000148 Bar/Hz, and the microphone was 0.028 Bar/Hz with a standard error of 0.000132 Bar/Hz. The agreement of the calculated gradients further highlights the consistency between each detection technique. Albeit, only two isolated modes from the spectra have been analysed further, the experimental results shown in Figs. 8 and 9 clearly highlight the similarities between the measurements, and show a strong correlation between pressure and resonant mode frequency shifts. The application of a linear regression fit to each mode has enabled the characterisation of the Bar/Hz change, and shows it is possible to measure the pressure of the SNM containment through monitoring the resonant frequency shifts of different modes within the spectra.

5. Conclusion

A non-contact acoustic resonance technique has been developed that measures frequency changes, attributed to an increase in internal pressure of a welded stainless steel sealed package. A wideband EMAT has been used to excite the vibrational resonant modes of an SNM containment, and analysis performed in the frequency domain has identified the shift of vibrational resonant modes for increasing internal pressure of the containment. Both EMAT and microphone detection techniques show agreement in the vibrational resonant frequencies that are detected. It should be noted that the data set is limited and shows a complex relationship between containment internal pressure, material elasticity and changes to the vibrational resonant frequencies. This points to the possibility of using machine learning to aid with analysis for a deeper understanding, where there are many more modes present in the data.

Future work will include testing a non-deformed Magnox can with both the EMAT and microphone techniques, to understand the vibrational resonant frequency response of the containment for within the elastic limit. Additional testing on Magnox cans of different internal

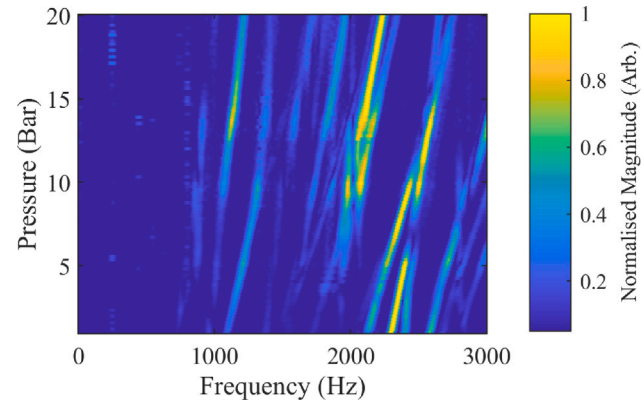

Fig. 10. Reduced frequency range image plot for EMAT detection method. The dynamic range of the normalised magnitude colour bar has been adjusted to enhance the low frequency (below 3 kHz) spectral components. (For interpretation of the references to colour in this figure legend, the reader is referred to the web version of this article.)

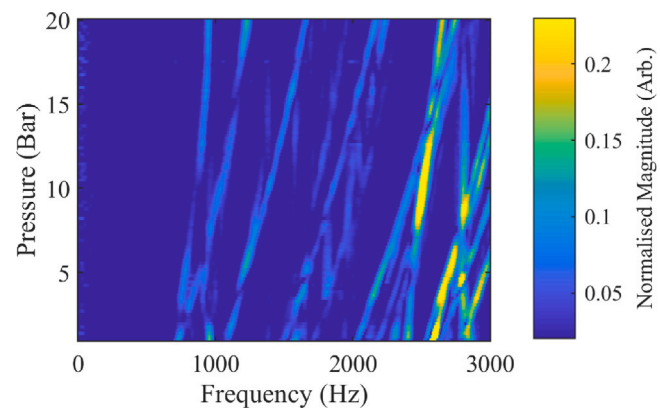

Fig. 11. Reduced frequency range image plot for microphone detection method. The dynamic range of the normalised magnitude colour bar has been adjusted to enhance the low frequency (below 3 kHz) spectral components. (For interpretation of the references to colour in this figure legend, the reader is referred to the web version of this article.)

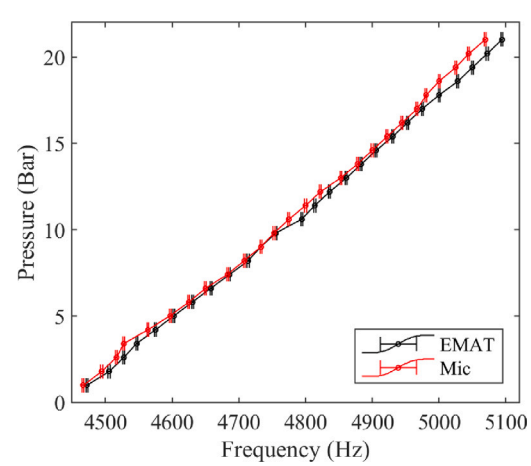

Fig. 12. Resonant frequency variation of one isolated mode at approximately 4400 Hz with pressure, extracted from the EMAT and microphone image plots.

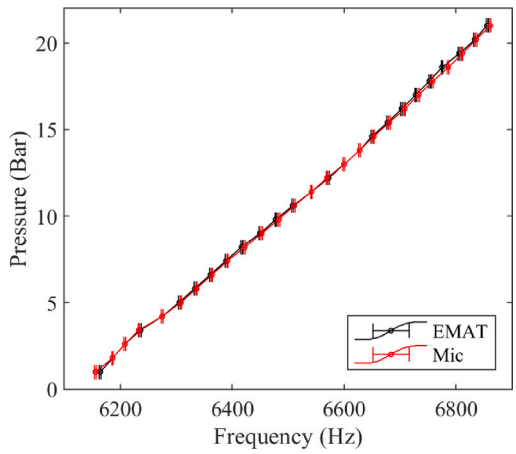

Fig. 13. Resonant frequency variation of one isolated mode at approximately 6100 Hz with pressure, extracted from the EMAT and mic image plots.

fill masses will provide an understanding of the can to can variation, that will be expected within the storage facilities, and how internal mass changes are reflected within the vibrational response of the can. Finite element models will be constructed to investigate the vibrational resonant frequencies and corresponding modes shapes of the containment wall. This will assist in identifying any potential modes that may be beneficial to excite in preference to others, and if the placement of the excitation transducer on the containment wall is essential for the excitation of a particular mode. Theoretical and analytical modelling of the predicted resonant frequencies is not possible for such a complex shaped structure and would add no additional insight beyond the finite element modelling. The temperature of the Magnox cans are known to increase while in the storage facilities, therefore it is essential to perform testing on the SNM containment for different temperatures in future work, to understand the effect of temperature on pressure and the vibrational frequency modes.

Declaration of competing interest

The authors declare that they have no known competing financial interests or personal relationships that could have appeared to influence the work reported in this paper.

Data availability

The data that has been used is confidential.

References

[1] Nuclear PEW. 2019 UK radioactive material inventory. Technical report, Cumbria, UK: Nuclear Decommissioning Authority; 2019.
[2] Authority ND. Progress on plutonium consolidation, storage and disposition. Technical report, Cumbria, UK: Nuclear Decommissioning Authority; 2019.
[3] Verma V, Katovsky K. Spent nuclear fuel and accelerator-driven sub-critical systems. Singapore: Springer Nature; 2019.
[4] Government U. Nuclear decommissioning authority strategy. Technical report, Cumbria, UK: Nuclear Decommissioning Authority; 2021.
[5] IAEA. IAEA nuclear energy series no. NG-T-3.20 24. 2019.
[6] Hyatt NC. Safe management of the UK separated plutonium inventory: a challenge of materials degradation. NPJ Mater Degrad 2020;4(1):1–4.
[7] Sims HE, Webb KJ, Brown J, Morris D, Taylor RJ. Hydrogen yields from water on the surface of plutonium dioxide. J Nucl Mater 2013;437(1–3):359–64.
[8] Ohtani T, Ogi H, Hirao M. Electromagnetic acoustic resonance to assess creep damage in Cr-Mo-V steel. Jpn J Appl Phys 1: Regular Pap Short Not Rev Pap 2006;45(5 B):4526–33.
[9] Hirao M, Ogi H. Electromagnetic acoustic transducers: noncontacting ultrasonic measurements using EMATs. Osaka, Japan: Springer Tokyo; 2017.
[10] Atkinson I, Gregory C, Kelly SP, Kirk KJ. Ultrasmart: Developments in ultrasonic flaw detection and monitoring for high temperature plant applications. In: Eighth international conference on creep and fatigue at elevated temperatures. Pressure vessels and piping conference, vol. 9, 2007, p. 573–85.
[11] Hirao M, Ogi H, Fukuoka H. Resonance EMAT system for acoustoelastic stress measurement in sheet metals. Rev Sci Instrum 1993;64(11):3198–205.
[12] Hirao M, Ogi H. Electromagnetically excited acoustic resonance for evaluating attenuation coefficient and grain size in polycrystalline metals. Appl Phys Lett 1994;64(17):2217–9.
[13] Dixon S, Edwards C, Palmer S. Texture measurements of metal sheets using wideband electromagnetic acoustic transducers. J Phys D: Appl Phys 2002;35:816.
[14] Jian X, Dixon S, Edwards RS, Reed J. Coupling mechanism of electromagnetic acoustical transducers for ultrasonic generation. J Acoust Soc Am 2006;119(5):2693–701.
[15] Norton MP, Karczub DG. Noise and vibration as a diagnostic tool. 2012, p. 488–565.
[16] Jian X, Dixon S. Enhancement of EMAT and eddy current using a ferrite back-plate. Sensors Actuators A 2007;136(1):132–6.
[17] Arduinocc. Arduino uno. 2010, https://www.arduino.cc.
[18] MathWorks. Matlab R2021a. 2021, https://www.mathworks.com.
[19] Dixon S, Fletcher M, Rowlands G. The accuracy of acoustic birefringence shear wave measurements in sheet metal. J Appl Phys 2008;104.